

---

# Conformal Prediction with Upper and Lower Bound Models

---

**Miao Li\***

ISyE, Georgia Institute of Technology  
Atlanta, GA 30332  
miao.li@gatech.edu

**Michael Klamkin**

ISyE, Georgia Institute of Technology  
Atlanta, GA 30332  
klam@isye.gatech.edu

**Mathieu Tanneau**

ISyE, Georgia Institute of Technology  
Atlanta, GA 30332  
mathieu.tanneau@isye.gatech.edu

**Reza Zandehshahvar**

ISyE, Georgia Institute of Technology  
Atlanta, GA 30332  
reza@isye.gatech.edu

**Pascal Van Hentenryck**

ISyE, Georgia Institute of Technology  
Atlanta, GA 30332  
pascal.vanhentenryck@isye.gatech.edu

## Abstract

Decision makers routinely use optimization technology to plan and operate complex systems like global supply chains or power grids. In that context, practitioners face the challenge of assessing the *optimality gap* of a given solution, i.e., how optimal or sub-optimal said solution is. While constrained optimization algorithms generally provide such information in the form of so-called dual bounds, these bounds are often too loose to be informative. Therefore, decision makers must evaluate solution quality using their domain knowledge and experience, which is prone to errors and may lead to sub-optimal decisions. This paper addresses that challenge by providing estimates of solution quality in the form of prediction intervals, obtained via conformal prediction techniques. To that end, the paper introduces a general framework for conformal prediction with upper and lower bound predictors, which explicitly addresses the potential heteroskedasticity of either predictor via a model selection step. The paper also proposes a principled mechanism to avoid paradoxical miscoverage in cases where upper/lower predictors are both highly accurate. Finally, numerical experiments on large-scale problems found in industry demonstrate that the proposed approach achieves substantial reduction in interval width over several baseline methods.

## 1 Introduction

Optimization technology is instrumental in operating complex systems efficiently, from supply chains, logistics and manufacturing to healthcare and power systems. Nevertheless, it is often intractable to obtain optimal solutions to large-scale, nonlinear and non-convex problems found in industry. This limitation has motivated the use of approximate and heuristic algorithms, which are fast but may return sub-optimal solutions. As a consequence, decision makers face the hurdle of assessing whether a given solution is optimal enough, or whether substantial improvements are possible. This

---

\*Corresponding author.

assessment requires computing *dual bounds*, i.e., mathematical certificates of solution quality, which are typically obtained by solving relaxations Boyd and Vandenberghe [2004], Geoffrion [2009] or by branch-and-bound algorithms Wolsey and Nemhauser [1999]. However, in real-life applications, these dual bounds may be too loose to be informative, thus leaving practitioners to evaluate solution quality by relying on their domain knowledge and experience, which is prone to errors and may lead to sub-optimal decisions.

To address this challenge, this paper proposes a data-driven approach that evaluates the sub-optimality of a solution by leveraging uncertainty quantification (UQ) and conformal prediction (CP) techniques. Namely, the paper proposes to provide probabilistic guarantees for solution quality in the form of prediction intervals. To the best of the authors' knowledge, this paper is the first to propose the use of CP to estimate solution sub-optimality in an optimization setting. In doing so, the paper introduces CPUL, a general framework for CP with upper and lower bounds. This contrasts with existing approaches from the optimization literature, which almost exclusively rely on computing valid, but possibly loose, dual bounds. The paper's setting also contrasts with traditional CP settings that rely on approximate predictors, e.g., mean predictors Vovk et al. [2005] or quantile regression models Romano et al. [2019] which, in the present setting, may not yield valid lower/upper bounds.

The paper's contributions are summarized as follows: (1) it presents a data-driven methodology to evaluate the optimality of solutions to optimization problems using uncertainty quantification techniques, (2) it introduces CPUL, a general framework for CP with upper and lower bounds, with a focus on capturing the heteroskedasticity of lower and upper bound residuals, (3) it addresses the paradox of miscoverage despite high-quality lower and upper bounds by proposing an additional mechanism, Optimal Minimum Length Threshold (OMLT), (4) it conducts numerical experiments on large-scale economic dispatch problems used in real-time electricity markets.

## 1.1 Problem statement

**Motivating Example** Consider a parametric optimization problem of the form

$$\Phi(x) = \min_s f_x(s) \tag{1a}$$

$$\text{s.t. } g_x(s) \leq 0, \tag{1b}$$

where  $x \in \mathcal{X} \subseteq \mathbb{R}^p$  denotes the instance's parameters,  $s \in \mathbb{R}^n$  are decision variables,  $f_x : \mathbb{R}^m \rightarrow \mathbb{R}$  is the objective function to be minimized,  $g_x : \mathbb{R}^n \rightarrow \mathbb{R}^m$  encodes constraints and  $\mathcal{S}_x = \{g_x(s) \leq 0\}$  is the set of feasible solutions, and  $\Phi(x)$  is the instance's optimal value. The paper assumes the availability of a primal-dual pair in the following form. A *primal* solution  $\bar{s} \in \mathcal{S}_x$  provides a primal (upper) bound on the optimal value, i.e.,  $f_x(\bar{s}) \geq \Phi(x)$ . Primal solutions are obtained using either heuristics or exact algorithms. Conversely, a *dual* (lower) bound  $\psi \in \mathbb{R}$  is guaranteed to be smaller than the optimal value, i.e.,  $\psi \leq \Phi(x)$ . Dual bounds are obtained from relaxations and/or branch-and-bound algorithms, and provide a mathematical certificate on the quality of a primal solution  $\bar{s}$ . It is important to note that all modern global optimization algorithms return such a primal-dual pair. It is also possible to obtain a primal-dual pair using only machine learning (ML) models, by combining primal-feasible ML architectures Dotti et al. [2021], Chen et al. [2023] with the dual lagrangian learning framework introduced in Tanneau and Hentenryck [2024].

**General problem setting** Consider a random variable  $X$  with support  $\mathcal{X} \subseteq \mathbb{R}^d$ , and an unknown Borel measurable function  $f: \mathcal{X} \rightarrow \mathbb{R}$  that defines a target  $Y = f(X) \in \mathbb{R}$ . Let  $\hat{B}^l$  and  $\hat{B}^u$  be given lower and upper predictors for  $f$ , i.e.,

$$\forall x \in \mathbb{R}^d, \hat{B}^l(x) \leq f(x) \leq \hat{B}^u(x). \tag{2}$$

These predictors inherently form a 100% prediction interval  $[\hat{B}^l(X), \hat{B}^u(X)]$  for  $Y$ . Recall that, in a constrained optimization context, upper and lower predictors are obtained from primal and dual information, respectively. The goal of this paper is to derive tighter prediction intervals by targeting a  $(1 - \alpha)$  marginal coverage for  $Y$  (where  $\alpha \in [0, 1]$ ), rather than perfect coverage.

Formally, consider a dataset of  $N$  independent and identically distributed (i.i.d.) observations  $(X_i, Y_i)_{i \in [N]}$ , where  $X_i$  is sampled from an underlying distribution  $\mathcal{P}$ , and  $Y_i = f(X_i), \forall i \in [N]$ . Following the standard procedure of the split CP framework Vovk et al. [2005], divide the  $N$  samples into a training and a calibration set, denoted as  $\mathcal{D}_{\text{train}}$  and  $\mathcal{D}_{\text{cal}}$ , with corresponding indices  $\mathcal{I}_{\text{train}}, \mathcal{I}_{\text{cal}}$ .

Next, consider a new i.i.d. observation  $X_{N+1}$ , sampled from  $\mathcal{P}$ . For  $\alpha \in [0, 1]$ , the goal is to refine the initial prediction interval  $\tilde{C}(X_{N+1}) = [\hat{B}^l(X_{N+1}), \hat{B}^u(X_{N+1})]$  into a (smaller) prediction interval  $\hat{C}(X_{N+1}) = [\hat{L}(X_{N+1}), \hat{U}(X_{N+1})]$  that satisfies the marginal coverage guarantee

$$\mathbb{P}(Y_{N+1} \in \hat{C}(X_{N+1})) \geq 1 - \alpha. \quad (3)$$

Indeed, recall that, while  $\tilde{C}(X_{N+1})$  has 100% coverage by construction, it may be too wide to derive meaningful insights. This motivates the need to derive smaller prediction intervals while ensuring reasonable marginal coverage. Then the goal can be restated as the optimization problem

$$\min_{\hat{C}} \mathbb{E}_{X \sim \mathcal{P}} [\hat{C}(X)] \quad (4a)$$

$$\text{s.t. } \mathbb{P}(f(X) \in \hat{C}(X)) \geq 1 - \alpha, \quad (4b)$$

where  $\hat{C}$  maps  $X \in \mathbb{R}^d$  to a subset of  $\mathbb{R}$ .

**Remark 1.** When multiple bounds  $\{\hat{B}_1^l, \dots, \hat{B}_{B_l}^l\}$  and  $\{\hat{B}_1^u, \dots, \hat{B}_{B_u}^u\}$  are provided, valid predictors  $\hat{B}^l(x)$  and  $\hat{B}^u(x)$  leveraging all this information effectively can be defined as

$$\hat{B}^l(x) = \max\{\hat{B}_1^l(x), \dots, \hat{B}_{B_l}^l(x)\}, \quad \hat{B}^u(x) = \min\{\hat{B}_1^u(x), \dots, \hat{B}_{B_u}^u(x)\}. \quad (5)$$

## 2 Background

UQ is crucial for informed decision making, particularly in real-world applications where prediction sets are preferred over point estimates. CP, first proposed by Vovk et al. [2005], is a widely used distribution-free UQ method, valued for its finite-sample coverage guarantees and computational efficiency. This section presents standard CP techniques, including Split CP, Conformal Quantile Regression, and Nested CP. While these methods can be applied to the problem at hand (see Section 5 and Appendix B.4.1), unlike the proposed framework, they are not designed to explicitly leverage valid lower and upper bound predictors.

**Split Conformal Prediction (SCP)** Vovk et al. [2005], Papadopoulos et al. [2002], Lei et al. [2018] is one of the most commonly used CP frameworks. Therein, a mean prediction model  $\hat{f}$  is first trained using the training data  $\mathcal{D}_{train}$ . SCP then produces prediction intervals of the form

$$\hat{C}_{SCP}(x) = \left\{ y \mid \hat{Q}_{\frac{\alpha}{2}}^{SCP} \leq \hat{s}(x, y) \leq \hat{Q}_{1-\frac{\alpha}{2}}^{SCP} \right\}, \quad (6)$$

where  $\hat{s} : \mathbb{R}^d \times \mathbb{R} \rightarrow \mathbb{R}$  is a so-called *conformity score*, and  $\hat{Q}_{\frac{\alpha}{2}}^{SCP}, \hat{Q}_{1-\frac{\alpha}{2}}^{SCP}$ , denote the empirical  $\frac{\alpha}{2}$  and  $1 - \frac{\alpha}{2}$  quantiles of the scores  $\{\hat{s}(X_i, Y_i)\}_{i \in \mathcal{I}_{cal}}$ . Under the exchangeability assumption, the resulting prediction intervals have valid marginal coverage Vovk et al. [2005], i.e.,

$$\mathbb{P}_{X_{N+1} \sim \mathcal{P}} (Y_{N+1} \in \hat{C}_{SCP}(X_{N+1})) \geq 1 - \alpha. \quad (7)$$

Common choices of conformity scores include the residual score  $\hat{s}(x, y) = y - \hat{f}(x)$  and the absolute residual score  $\hat{s}(x, y) = |y - \hat{f}(x)|$ ; the reader is referred to Angelopoulos and Bates [2021], Oliveira et al. [2024] for a more exhaustive review of SCP and conformity scores. The SCP methodology can be applied to the paper's setting by replacing  $\hat{f}$  in the above construction with either the lower ( $\hat{B}^l$ ) or upper bound ( $\hat{B}^u$ ) predictor. However, this fails to jointly utilize information from both bounds.

**Conformal Quantile Regression (CQR)** To alleviate SCP's lack of local adaptivity, CQR Romano et al. [2019] combines quantile regression models with a conformalization procedure: First, CQR trains quantile regression models to predict the quantiles  $\alpha_{lo}$  and  $\alpha_{hi}$ . Then, conformalize as follows

$$\hat{C}^{CQR}(x) = \left[ \hat{q}_{\alpha_{lo}}(x) - \hat{Q}_{1-\alpha}^{CQR}, \hat{q}_{\alpha_{hi}}(x) + \hat{Q}_{1-\alpha}^{CQR} \right], \quad (8)$$

where  $\hat{q}_{\alpha_{lo}}(x), \hat{q}_{\alpha_{hi}}(x)$  are the predicted lower and upper quantiles given input data  $x$ , and  $\hat{Q}_{1-\alpha}^{CQR}$  is the  $1 - \alpha$  quantile of the conformity scores  $\{\hat{s}^{CQR}(X_i, Y_i)\}_{i \in \mathcal{I}_{cal}}$ , defined as

$$\hat{s}^{CQR}(x, y) = \max(\hat{q}_{\alpha_{lo}}(x) - y, y - \hat{q}_{\alpha_{hi}}(x)). \quad (9)$$

The CQR method could be adapted to the setting at hand by approximating  $\hat{q}_{\alpha_{lo}}, \hat{q}_{\alpha_{hi}}$  with  $\hat{B}^l, \hat{B}^u$  in the above derivation. Unlike the standard CQR, which requires fitting auxiliary quantile regression models whose accuracy dictates performance (and may require large training datasets in high-dimensional settings),  $\hat{B}^l, \hat{B}^u$  from the constrained optimization formulation offer key advantages. These bounds are often directly computable from the base model (e.g., once a feasible primal model is constructed, an upper bound can be computed by evaluating the objective at that solution), making them available at minimal cost. They also inherently guarantee perfect coverage, regardless of training data size. This paper focuses on effectively leveraging these readily available and valid bounds.

**Nested Conformal Prediction (NCP)** Gupta et al. [2022] introduces a unifying CP framework by nested prediction sets. NCP considers a family of nested prediction intervals  $\{\hat{C}_t\}_{t \in \mathcal{T} \subseteq \mathbb{R}}$ , i.e.,

$$\forall x \in \mathcal{X}, \forall t \leq t', \hat{C}_t(x) \subseteq \hat{C}_{t'}(x), \quad (10)$$

and such that  $\hat{C}_{\inf(\mathcal{T})} = \emptyset$  and  $\hat{C}_{\sup(\mathcal{T})} = \mathbb{R}$ . Then, prediction intervals are of the form  $\hat{C}^{\text{NCP}}(x) = \hat{C}_\tau(x)$ , where

$$\tau = \inf_{t \in \mathcal{T}} \left\{ t \left| \sum_{i \in \mathcal{I}_{\text{cal}}} \mathbf{1}_{\hat{C}_t(X_i)}(Y_i) \geq (1-\alpha)(1+|\mathcal{I}_{\text{cal}}|) \right. \right\} \quad (11)$$

is computed from the calibration set. This framework encompasses all types of conformity scores, while maintaining the theoretical guarantees of standard CP Gupta et al. [2022]. For instance, the CQR construction can be cast in the NCP framework by considering

$$\hat{C}_t(x) = [\hat{q}_{\frac{\alpha}{2}}(x) - t, \hat{q}_{1-\frac{\alpha}{2}}(x) + t]. \quad (12)$$

To ensure clarity, the remainder of the paper is presented using the NCP framework. Namely, each CP methodology is presented by stating the corresponding family of nested prediction sets; prediction intervals are then constructed using the NCP approach and Eq. (11).

**Other Related Methods** CP techniques have been used to analyze the precision of sketching algorithms, which are increasingly vital tools for handling massive datasets in modern machine learning Broder and Mitzenmacher [2004], Goyal et al. [2012], Cormode et al. [2018], Zhang et al. [2014]. Sesia et al. [2023] construct prediction intervals for the frequency of a queried object based on a sketch Charikar et al. [2002]. Therein, a deterministic upper bound  $\hat{B}^u$  provided by Cormode and Muthukrishnan [2005] is combined with a trivial lower bound  $\hat{B}^l = 0$  (reflecting the non-negativity of counts) to construct nested intervals. The construction, referred to as “SFD CP” in this paper, is defined as:

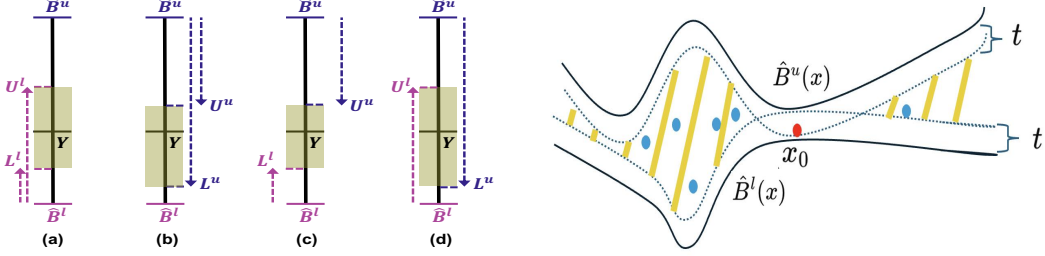
$$\hat{C}_t^{\text{SFD}}(x) = [\max\{0, \hat{B}^u(x) - t\}, \min\{\hat{B}^u(x), t\}]. \quad (13)$$

Sesia et al. [2023] also introduces an adaptive version of this construction, designed to better account for heteroscedasticity in residuals. The CPUL framework generalizes this approach by combining information from  $\hat{B}^l, \hat{B}^u$  in multiple ways; see Section 3.2.

Another related line of work leverages information from multiple models fitted on the training set. For example, Liang et al. [2024], Yang and Kuchibhotla [2024] focus on selecting the model that produces the most efficient prediction intervals. Extending these ideas, the CPUL framework reinterprets the problem in the context of multiple models, simultaneously utilizing both upper and lower bounds to maximize the utility of the available information.

### 3 CP With Upper And Lower Bounds

This section presents CPUL, designed to exploit the strong properties of  $\hat{B}^l, \hat{B}^u$ . A key limitation of traditional CP methods like SCP and CQR is not leveraging that  $\hat{B}^l, \hat{B}^u$  yield valid lower and upper bounds on the target variable. Additionally, these methods do not necessarily integrate information from both models nor are they inherently designed to account for heteroskedastic residuals between these bounds (e.g.,  $\hat{B}^l$  might provide accurate estimates while  $\hat{B}^u$  performs poorly). The results in Section 5 further validate these observations.



(a) Illustration of the construction of prediction intervals in CPUL: (a)  $\hat{C}_0^{\text{ll}}$ , (b)  $\hat{C}_0^{\text{uu}}$ , (c)  $\hat{C}_0^{\text{lu}}$ , (d)  $\hat{C}_0^{\text{ul}}$ . Each family of prediction intervals is conformed following the NCP framework (see Eq. (11)).

(b) Illustration of Paradoxical Miscoverage (motivation for OMLT): using a constant offset ( $\pm t$ ) in the NCP construction results in an empty prediction interval where  $\hat{B}^u(x) - \hat{B}^l(x)$  is small.

Figure 1: Illustration of CPUL-OMLT construction

### 3.1 Exploiting valid bounds in NCP

Recall that  $\hat{B}^l, \hat{B}^u$  provide valid lower and upper bounds on the target variable, i.e.,  $\hat{B}^l(X) \leq Y \leq \hat{B}^u(X)$  always holds. This suggests a simple procedure for strengthening  $\hat{C}$  without loss of coverage (as shown by Proposition 1) into

$$\tilde{C}(x) = \hat{C}(x) \cap [\hat{B}^l(x), \hat{B}^u(x)]. \quad (14)$$

**Proposition 1.** Let  $\hat{C}(\cdot)$  denote a prediction interval with coverage  $1 - \alpha$ , i.e.,  $\mathbb{P}(Y_{N+1} \in \hat{C}(X_{N+1})) = 1 - \alpha$  for some  $\alpha \in [0, 1]$ . Next, define the strengthened interval  $\tilde{C}(x) := \hat{C}(x) \cap [\hat{B}^l(x), \hat{B}^u(x)], \forall x \in \mathcal{X}$ . Then,  $\mathbb{P}(Y_{N+1} \in \tilde{C}(X_{N+1})) = \mathbb{P}(Y_{N+1} \in \hat{C}(X_{N+1})) = 1 - \alpha$ .

It is important to note that Proposition 1 holds irrespective of how the original prediction interval  $\hat{C}$  is obtained. Theorem 1 shows that, if the calibration step is performed using the NCP framework, then there is no loss of performance whether the strengthening is performed before or after calibration.

**Theorem 1.** Consider a family of nested prediction sets  $\{\hat{C}_t\}_{t \in \mathcal{T}}$ , where  $\mathcal{T} \subseteq \mathbb{R}$ , and let  $\hat{\tau}$  be obtained following the NCP calibration step as per Eq. (11). Next, define the family of nested strengthened intervals  $\{\tilde{C}_t\}_{t \in \mathcal{T}}$ , where  $\forall x \in \mathbb{R}^d, \forall t \in \mathcal{T}, \tilde{C}_t(x) = \hat{C}_t(x) \cap [\hat{B}^l(x), \hat{B}^u(x)]$ , and let  $\tilde{\tau}$  be obtained from Eq. (11). Then,  $\hat{\tau} = \tilde{\tau}$  and  $\forall x \in \mathbb{R}^d$ ,

$$\hat{C}_{\hat{\tau}}(x) \cap [\hat{B}^l(x), \hat{B}^u(x)] = \tilde{C}_{\tilde{\tau}}(x). \quad (15)$$

Theorem 1 allows to decouple the calibration step from the strengthening. Thereby, one can perform the calibration step without access to  $\hat{B}^l$  or  $\hat{B}^u$ , without any loss of coverage. This is particularly valuable when  $\hat{B}^l$  or  $\hat{B}^u$  are not available during training/calibration due to, e.g., privacy concerns.

### 3.2 The CPUL approach

The proposed CPUL framework combines several steps to fully exploit the knowledge that  $\hat{B}^l$  and  $\hat{B}^u$  provide valid bounds on the target variable, and to account for the heteroskedasticity of their residuals. The algorithm is presented in the NCP framework and, for ease of reading, the presentation omits the strengthening of prediction intervals described in Eq. (14), i.e., strengthening is always performed implicitly. Recall that, by Theorem 1, this does not affect the conformation procedure.

First define the residuals  $\hat{r}^l = Y - \hat{B}^l(X)$  and  $\hat{r}^u = Y - \hat{B}^u(X)$ , and denote by  $\hat{Q}_\beta^l, \hat{Q}_\beta^u$  the  $\beta$  quantiles of  $\hat{r}^l, \hat{r}^u$ , evaluated on the training set. Then define

$$L^l(x) = \hat{B}^l(x) + \hat{Q}_{\frac{\alpha}{2}}^l, \quad (16a)$$

$$L^u(x) = \hat{B}^u(x) + \hat{Q}_{\frac{\alpha}{2}}^u, \quad (16b)$$

$$U^l(x) = \hat{B}^l(x) + \hat{Q}_{1-\frac{\alpha}{2}}^l, \quad (16c)$$

$$U^u(x) = \hat{B}^u(x) + \hat{Q}_{1-\frac{\alpha}{2}}^u. \quad (16d)$$

Note that  $L^l, L^u, U^l, U^u$  do not provide valid lower nor upper bounds on the target variable ( $Y$ ). The motivation for adjusting the initial predictors  $\hat{B}^l, \hat{B}^u$  using quantiles  $\hat{Q}^l, \hat{Q}^u$  is to account for the

---

**Algorithm 1** CPUL

---

**Input:**  $\mathcal{D} = (X_i, Y_i)_{i=1}^N$ ,  $\alpha \in [0, 1]$ . **Output:** Selected model  $\hat{C}^{**}$ .

- 1: Split  $\mathcal{D}$  into training and calibration sets  $\mathcal{D}_{\text{train}}$  and  $\mathcal{D}_{\text{cal}}$
- 2: Train lower/upper bound models  $\hat{B}^l, \hat{B}^u$  using  $\mathcal{D}_{\text{train}}$
- 3: Compute empirical quantiles  $\hat{Q}_{\frac{\alpha}{2}}^l, \hat{Q}_{1-\frac{\alpha}{2}}^l, \hat{Q}_{\frac{\alpha}{2}}^u, \hat{Q}_{1-\frac{\alpha}{2}}^u$  on the training set  $\mathcal{D}_{\text{train}}$
- 4: Form  $\{\hat{C}_t^{\text{ll}}\}_{t \in \mathbb{R}}, \{\hat{C}_t^{\text{lu}}\}_{t \in \mathbb{R}}, \{\hat{C}_t^{\text{ul}}\}_{t \in \mathbb{R}}, \{\hat{C}_t^{\text{uu}}\}_{t \in \mathbb{R}}$  as per Eq. (17), and compute  $\tau^{\text{ll}}, \tau^{\text{lu}}, \tau^{\text{ul}}, \tau^{\text{uu}}$  using Eq. (11).
- 5: Select model with smallest width on calibration set

$$\hat{C}^{**} := \underset{\hat{C} \in \{\hat{C}_{\tau^{\text{ll}}}^{\text{ll}}, \hat{C}_{\tau^{\text{lu}}}^{\text{lu}}, \hat{C}_{\tau^{\text{ul}}}^{\text{ul}}, \hat{C}_{\tau^{\text{uu}}}^{\text{uu}}\}}{\operatorname{argmin}} \frac{1}{|\mathcal{D}_{\text{cal}}|} \sum_{X_i \in \mathcal{D}_{\text{cal}}} |\hat{C}(X_i)|$$


---

heteroskedascity of  $\hat{r}^l, \hat{r}^u$ . Also note that the construction in Eq. (16) only requires evaluating the residuals  $\hat{r}^l, \hat{r}^u$  on the training set, and extracting their quantiles.

Next,  $L^l, L^u, U^l, U^u$  are combined to form four families of nested prediction intervals  $\{\hat{C}_t^{\text{ll}}\}_{t \in \mathbb{R}}, \{\hat{C}_t^{\text{lu}}\}_{t \in \mathbb{R}}, \{\hat{C}_t^{\text{ul}}\}_{t \in \mathbb{R}}, \{\hat{C}_t^{\text{uu}}\}_{t \in \mathbb{R}}$  as follows:

$$\hat{C}_t^{\text{ll}}(x) = [L^l(x) - t, U^l(x) + t], \quad (17a)$$

$$\hat{C}_t^{\text{lu}}(x) = [L^l(x) - t, U^u(x) + t], \quad (17b)$$

$$\hat{C}_t^{\text{ul}}(x) = [L^u(x) - t, U^l(x) + t], \quad (17c)$$

$$\hat{C}_t^{\text{uu}}(x) = [L^u(x) - t, U^u(x) + t]. \quad (17d)$$

This construction is illustrated in Figure 1a. Each family is then conformalized using the NCP procedure on the calibration set, and the model with smallest width is selected.

Algorithm 1 summarizes the proposed CPUL method, which proceeds as follows. First, the dataset  $\mathcal{D}$  is split into training and calibration sets (line 1). Then, lower and upper bound predictors (i.e.,  $\hat{B}^l, \hat{B}^u$ ) are trained using the training set (line 2), after which quantiles of the corresponding residuals are evaluated on the training set (line 3). Next, four families of nested intervals are constructed following Eq. (17), each of which is calibrated using the NCP framework (Eq. (11)) and the calibration set  $\mathcal{D}_{\text{cal}}$  (line 4). The final step of the algorithm (line 5) selects, among the four models  $\hat{C}^{\text{ll}}, \hat{C}^{\text{lu}}, \hat{C}^{\text{ul}}, \hat{C}^{\text{uu}}$ , the one with smallest average width over the calibration set (as an estimator of  $\mathbb{E}|\hat{C}(X_{N+1})|$ ). It is important to note that the model selection step is not performed on a per-sample basis. Rather, Algorithm 1 selects *one* variant among  $\hat{C}^{\text{ll}}, \hat{C}^{\text{lu}}, \hat{C}^{\text{ul}}, \hat{C}^{\text{uu}}$ , which is then used across the entire test set. For instance, if  $\hat{C}_{\tau^{\text{lu}}}^{\text{lu}}$  is selected, then  $\hat{C}^{**} = \hat{C}_{\tau^{\text{lu}}}^{\text{lu}}$  and the CPUL prediction interval is  $\hat{C}^{**}(X_{N+1}) = \hat{C}_{\tau^{\text{lu}}}^{\text{lu}}(X_{N+1})$ . Theorem 2 provides theoretical guarantees on the coverage of  $\hat{C}^{**}$ .

**Theorem 2.** Assume that  $\{(X_1, Y_1), \dots, (X_{N+1}, Y_{N+1})\}$  are i.i.d. samples, and let  $\hat{C}^{**}$  be the CPUL model selected by Algorithm 1. Define  $N_{\text{cal}} = |\mathcal{D}_{\text{cal}}|$  and  $\eta = \sqrt{\log(8)/2} + 1/3$ . Then

$$\mathbb{P}\left(Y_{N+1} \in \hat{C}^{**}(X_{N+1})\right) \geq \frac{1+N_{\text{cal}}}{N_{\text{cal}}} (1-\alpha) - \frac{\eta}{\sqrt{N_{\text{cal}}}}. \quad (18)$$

*Proof.* The result follows directly from Theorem 1 from Yang and Kuchibhotla [2024].  $\square$

### 3.3 Relation to other methods

Several parallels can be drawn between CPUL and existing CP methodologies. For instance, the use of residual quantiles  $\hat{Q}^l, \hat{Q}^u$ , when constructing the nested prediction sets  $\hat{C}^{\text{ll}}, \hat{C}^{\text{uu}}$ , is related to the Split CP method. Indeed, applying SCP to  $\hat{B}^l$  or  $\hat{B}^u$  yields conformal prediction intervals (see Eq. (6)) that closely resemble the structure of  $\hat{C}^{\text{ll}}$  and  $\hat{C}^{\text{uu}}$ . Therefore, given that CPUL also exploits the  $\hat{C}^{\text{lu}}$  and  $\hat{C}^{\text{ul}}$  variants, one should expect CPUL to consistently outperform either SCP baseline.

The  $\hat{C}^{\text{ul}}$  construction is also related to the adaptive approach followed in Sesia et al. [2023]. The main difference between the two is the use of empirical quantiles  $\hat{Q}^l, \hat{Q}^u$  in CPUL, which can be obtained much more efficiently, compared to training additional quantile regression models as in Sesia et al. [2023]. The latter approach provides finer local adaptivity, albeit at a higher computational cost.

## 4 Optimal Minimal Length Threshold

A key limitation of CPUL, like most well-known CP methods, is its tendency to produce overly narrow prediction intervals, particularly when the initial bounds  $\hat{B}^u(x)$  and  $\hat{B}^l(x)$  are tight. The length of the prediction intervals in Eq. (16) scales with the magnitude of  $\hat{B}^u(x) - \hat{B}^l(x)$ . Consequently, when the bounds are extremely tight, the constant adjustment of  $t$  in the NCP framework becomes disproportionately large, leading empty prediction intervals and, in turn, under-coverage in such regions. Figure 1b illustrates this issue in the CPUL-lu setting. After calibrating the initial bounds the area around  $x_0$  remains uncovered due to the empty intersection of the calibrated intervals. This behavior results in inefficient prediction intervals, as the method should over-cover the less confident regions (i.e., areas where  $\hat{B}^u(x) - \hat{B}^l(x)$  is large). Hence, the regions with tightest initial bounds become most vulnerable and become under-covered. Sesia and Candès [2020] proposed a variant, CQR-r, with  $\hat{C}_t^{\text{CQR-r}}(x) = [\hat{L}_t^{\text{CQR-r}}(x), \hat{U}_t^{\text{CQR-r}}(x)]$ , for  $x \in \mathcal{X}$ , where

$$\hat{L}_t^{\text{CQR-r}}(x) = \hat{q}_{\alpha/2}(x) - t(\hat{q}_{1-\alpha/2}(x) - \hat{q}_{\alpha/2}(x));$$

$$\hat{U}_t^{\text{CQR-r}}(x) = \hat{q}_{1-\alpha/2}(x) + t(\hat{q}_{1-\alpha/2}(x) - \hat{q}_{\alpha/2}(x)).$$

The design of Sesia and Candès [2020] scales  $t$  by  $\hat{q}_{1-\alpha/2}(x) - \hat{q}_{\alpha/2}(x)$ , which mitigates the disproportionate reduction in prediction interval size. However, as noted in Sesia and Candès [2020], its overall efficiency is worse than the original fixed-length version (12). Thus, it remains unclear whether such scaling, despite being adaptive to the initial tightness of the base models, is preferred over the fixed-length adjustment  $t$ . Section 5 includes a CQR-r adaptation tailored to the setting of this paper for comparison.

To address this paradoxical miscoverage, the paper proposes the optimal minimal length threshold method (OMLT) as an alternative to the relative scaling approach used in Sesia and Candès [2020]. The core idea of OMLT consists in introducing a threshold  $\ell \geq 0$ , representing the minimum allowed length for a prediction interval. OMLT identifies regions where the given  $\hat{B}^u$  and  $\hat{B}^l$  are tightest, where even minor shrinking during calibration poses a high risk of significant undercoverage below the desired level of  $1 - \alpha$ . The design of OMLT retains the standard fixed-length adjustment of  $t$  and introduces a threshold for the minimal allowed prediction interval length, effectively marking the boundary of high-risk regions.

Consider a family of nested intervals  $\{\hat{C}_t\}_{t \in \mathcal{T}}$  satisfying the NCP assumptions, and define

$$\kappa_\ell(x) = \inf_{t \in \mathcal{T}} \{t \mid \ell \leq |\hat{C}_t(x)|\}, \quad (19)$$

from which a new family  $\{\bar{C}_t\}_{t \in \mathcal{T}}$  is constructed as

$$\bar{C}_{\ell,t}(x) = \begin{cases} \hat{C}_t(x) & \text{if } (\Delta(x) \geq \ell) \wedge (t > \kappa_\ell(x)) \\ \hat{C}_{\kappa_\ell(x)}(x) & \text{if } (\Delta(x) \geq \ell) \wedge (t \leq \kappa_\ell(x)) \\ [\hat{B}^l(x), \hat{B}^u(x)] & \text{if } (\Delta(x) \leq \ell) \end{cases} \quad (20)$$

where  $\Delta(x) = \hat{B}^u(x) - \hat{B}^l(x)$ . It is easy to verify that  $\{\bar{C}_{\ell,t}\}_{t \in \mathcal{T}}$  is a nested family, therefore satisfying the coverage guarantee given in (11). The minimum length threshold  $\ell$  may be specified by the user as a hyper-parameter, obtained as the solution of the optimization problem

$$\min_{\ell \geq 0, t \in \mathcal{T}} \mathbb{E}_X [|\bar{C}_{\ell,t}(X)|] \quad (21a)$$

$$\text{s.t. } \mathbb{P}(f(X) \in \bar{C}_{\ell,t}(X)) \geq 1 - \alpha. \quad (21b)$$

The key idea underlying OMLT is that the size of the prediction interval should not be smaller than  $\ell$ , which prevents under-coverage when a prediction interval is too small. The only exception is for the tightest regions, i.e., when  $\hat{B}^u(x) - \hat{B}^l(x) \leq \ell$ , in which case there is no need to enlarge  $\bar{C}_{\ell,t}(x)$  beyond  $\ell$ . The original upper and lower bounds can be confidently relied upon, as  $[\hat{B}^l(x), \hat{B}^u(x)]$  already provides high-quality coverage.

Since (21) reduces to the original problem in (4) when  $\ell = 0$  for arbitrary  $\{\hat{C}_t\}_{t \in \mathcal{T}}$ , the formulation of CPUL-OMLT is designed to produce prediction intervals whose expected length is generally not greater than that of CPUL, at the same  $1 - \alpha$  coverage. Moreover, OMLT has the potential to extend beyond this setting and reduce the average prediction interval length in cases where disproportionate prediction calibration is observed. For details of implementation, refer to Section B.4.2.

Table 1: Performance Comparison of CP Methods ( $\alpha = 10\%$ )

UQ Method	89_pegase		118_ieee		1354_pegase	
	PICP (%)	Size (%)	PICP (%)	Size (%)	PICP (%)	Size (%)
$[\hat{B}^l, \hat{B}^u]$	100.0 (0.00)	0.410 (0.016)	100.0 (0.00)	0.281 (0.085)	100.0 (0.00)	3.949 (3.807)
Split CP w/ $\hat{B}^l$	90.15 (0.60)	0.197 (0.007)	90.34 (0.63)	<b>0.206 (0.146)</b>	89.60 (0.54)	<b>1.308 (1.160)</b>
Split CP w/ $\hat{B}^u$	90.02 (0.54)	<b>0.205 (0.007)</b>	90.00 (0.50)	<b>0.105 (0.004)</b>	89.40 (0.49)	<b>1.570 (0.853)</b>
SFD CP	91.23 (0.56)	<b>0.188 (0.007)</b>	90.10 (0.50)	0.135 (0.013)	90.22 (0.27)	1.456 (0.609)
CQR	91.40 (1.80)	<b>0.389 (0.018)</b>	90.08 (2.75)	<b>0.190 (0.147)</b>	90.13 (0.43)	<b>3.501 (3.939)</b>
CQR-r	90.71 (0.72)	<b>0.332 (0.020)</b>	90.88 (1.33)	<b>0.180 (0.167)</b>	91.57 (1.32)	<b>3.271 (3.997)</b>
CPUL (ours)	91.23 (0.56)	<b>0.188 (0.007)</b>	90.02 (0.46)	<b>0.105 (0.004)</b>	89.65 (0.56)	<b>1.306 (1.162)</b>
CPUL-OMLT (ours)	90.28 (0.51)	<b>0.187 (0.008)</b>	90.01 (0.48)	<b>0.103 (0.007)</b>	89.69 (0.49)	<b>1.037 (0.890)</b>

<sup>\*</sup> For each dataset, the three shortest intervals are colored blue, while the three largest intervals are colored red.

## 5 Experiments

The performance of CPUL and CPUL-OMLT are evaluated to demonstrate their ability to achieve valid coverage while producing narrower prediction intervals. The experiments focus on UQ for the optimal value of economic dispatch problems, detailed in Appendix B.1. UQ is conducted given lower and upper bounds derived from primal-dual optimization proxy models Chen et al. [2023], Qiu et al. [2024], Klamkin et al. [2024], Chen et al. [2024]. Namely, the dual proxy provides valid lower bounds ( $\hat{B}^l$ ), and the primal proxy provides valid upper bounds  $\hat{B}^u$ ). Further details on these optimization proxies are provided in Appendices B.1 and B.3.

**Datasets** Experiments are performed over three datasets: 118\_ieee University of Washington, Dept. of Electrical Engineering [1999], 1354\_pegase Fliscounakis et al. [2013], and 89\_pegase Fliscounakis et al. [2013], corresponding to power grids of different sizes. For each dataset, samples are randomly shuffled and split 10 times. Dataset details are provided in Section B.2. Evaluation metrics reported are the mean and standard deviation across these 10 runs.

**Baselines** The performance of CPUL-OMLT is compared against several CP baselines. Recall that, unless specified otherwise, all prediction intervals are strengthened as per Eq. (14). The CP baselines include: Split CP (Eq. 6), using either  $\hat{B}^l$  or  $\hat{B}^u$  as base predictors; CQR and its variant CQR-r, wherein  $\hat{B}^l$  and  $\hat{B}^u$  are treated as the initial lower and upper quantile regressors in the CQR construction; an adapted SFP CP approach of Sesia et al. [2023]. Note that the latter matches the  $\hat{C}^{\text{ul}}$  construction. Additional implementation details are provided in Appendix B.4.1.

**Evaluation Metrics** All methods are evaluated on a held out test set  $\mathcal{D}_{\text{test}} = (X_i, Y_i)_{i \in \mathcal{I}_{\text{test}}}$ , using two evaluation criteria: *coverage* and *interval length*. The former is evaluated via the *Prediction Interval Coverage Percentage* (PICP), which measures the proportion of true values contained within the predicted intervals on the test set, i.e.,  $\text{PICP} = \frac{1}{|\mathcal{I}_{\text{test}}|} \sum_{i \in \mathcal{I}_{\text{test}}} \mathbf{1}_{\hat{C}(X_i)}(Y_i)$ .

At a given confidence level  $1 - \alpha$ , shorter interval lengths are considered more desirable. This is captured through *expected normalized length* of prediction interval  $\hat{C}$ , defined as  $\hat{E}_X(\hat{C}) = |\mathcal{I}_{\text{test}}|^{-1} \sum_{i \in \mathcal{I}_{\text{test}}} (|Y_i|^{-1} |\hat{C}(X_i)|)$ , where  $Y_i$  and  $\hat{C}(X_i)$  denote the (true) optimal value and the prediction interval for sample  $i$ . The paper considers the scaled interval length  $|\hat{C}(X_i)|/|Y_i|$ , expressed as a percentage, rather than absolute interval length  $|\hat{C}(X_i)|$ , to account for the possibly large range of values taken by  $Y$ . This metric is routinely used in the optimization literature Chen et al. [2023], Vivas et al. [2020], Wang et al. [2009], where it is referred to as *optimality gap*. All metrics are reported as the mean and standard deviation over 10 runs.

**Experiment Results** Table 1 and Figure 2 present the numerical performance of the various methods. Table 1 presents, for every dataset, the average and standard deviation of each method’s interval length and coverage, both expressed as a percentage. The table reports results for  $\alpha = 10\%$ ; additional  $\alpha$  values are reported in Table 3 in Appendix C. Figure 2 displays the interaction between each method’s interval length and coverage, across a broader range of  $\alpha$  values. This provides a more global view of each method’s overall performance.

The results in Table 1 demonstrate that all CP methods achieve satisfactory coverage levels, i.e., test coverage is typically close to  $1 - \alpha$ , which is expected given that all methods are properly

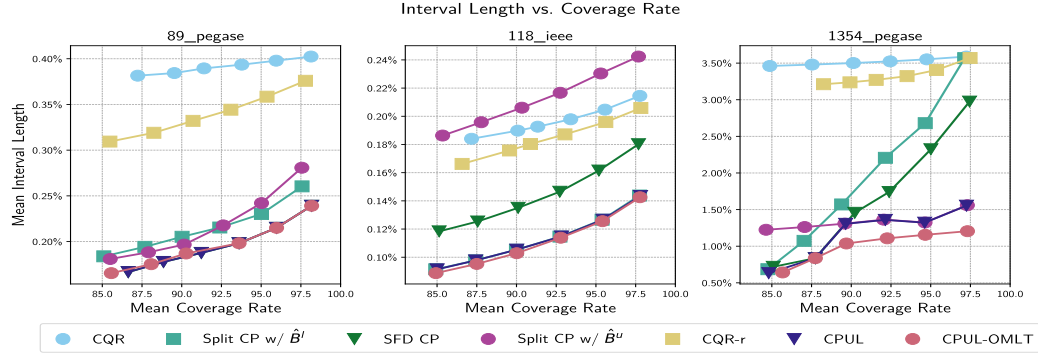


Figure 2: Performance comparison across datasets (Note: in 89\_pegase, SFD CP overlaps with CPUL and in 118\_ieee, Split CP w/  $\hat{B}^l$  overlaps with CPUL.)

calibrated. Moreover, all prediction intervals yield a substantial reduction in size compared to the original prediction  $[\hat{B}^l, \hat{B}^u]$ . For instance, a reduction of only 10% in coverage (i.e., 90% prediction intervals) can yield up to a two- and three-fold reduction in interval size. This demonstrates the value of using UQ techniques to provide more actionable information to practitioners.

Furthermore, CPUL and CPUL-OMLT consistently achieve state-of-the-art performance, across datasets and target coverage. On the other hand, CQR and CQR-r exhibit the worst performance overall, likely due to their inability to properly address heteroskedasticity. This is most evident in Figure 2. On the 1354\_pegase dataset (which corresponds to a larger power grid) CPUL-OMLT achieves the smallest interval size. In particular, CPUL-OMLT produces prediction intervals whose width is about 10% smaller than the second-best method, CPUL. These results highlight the important of the model selection procedure in CPUL.

Figure 2 demonstrates that, while methods like Split CP and SFD-CP deliver good results occasionally, their performance is highly variable across different datasets and confidence levels. For instance, although SFD-CP is among the best-performing methods on 89\_pegase, its performance on 1354\_pegase is significantly worse than CPUL when coverage is close to 100% (corresponding to small values of  $\alpha$ ). Similarly, Split CP using  $\hat{B}^u$  is among the worst performers on the 118\_IEEE dataset, but among the top performers on the 1354\_pegase dataset. Such variability in performance further reinforce the value of model selection, which is most evident on the 1354\_pegase dataset. Thereby, methods such as SCP with  $\hat{B}^l$  and SFP CP perform well when the coverage is between 85% and 90%, but are out-performed by SCP with  $\hat{B}^u$  when coverage is above 90%. In contrast, CPUL and CPUL-OMLT perform well across the entire coverage range. This is explained by the fact that CPUL and CPUL-OMLT select the best construction for *each target coverage  $\alpha$* .

Finally, while CPUL and CPUL-OMLT perform similarly on the 89\_pegase and 118\_IEEE datasets, CPUL-OMLT offers a clear improvement on the 1354\_pegase dataset, especially for coverage levels above 90% (see Figure 2). A more granular analysis of each model’s behavior reveals that CPUL’s performance is worse on samples where  $[\hat{B}^l, \hat{B}^u]$  is small. Namely, CPUL achieves a coverage of only about 50% across the 5% of test samples with smallest initial interval  $[\hat{B}^l, \hat{B}^u]$ . Recall that these samples correspond to regions where the given bounds  $\hat{B}^l, \hat{B}^u$  are the most accurate, which demonstrates the issue of paradoxical miscoverage (see Section 4 and Figure 1b). CPUL-OMLT effectively mitigates this issue, which results in better coverage and smaller interval length overall.

## 6 Conclusion

This paper introduced CPUL-OMLT, a novel CP mechanism designed for the settings that deterministic lower and upper bounds on the target variable are available. By integrating multiple interval construction strategies within the NCP framework, CPUL effectively leverages the structure of these bounds to improve efficiency. The OMLT mechanism leverages the strong condition that tight initial bounds already provide highly precise confidence intervals. Failure to account for this often leads to undercoverage in such regions, a challenge that existing methods struggle to address. Experimental validations were conducted on optimization problems across three power systems datasets, demonstrating that the proposed approach consistently outperforms the traditional CP methods by providing

better efficiency. The proposed CPUL-OMLT method provides state-of-the-art efficiency and remains consistent across different datasets, highlighting its robustness and practical relevance.

Future work could extend CPUL-OMLT beyond the efficient marginal coverage studied here. Potential directions include enforcing stronger conditional coverage to incorporate the already computed bounds  $\hat{B}^l, \hat{B}^u$ , integrating with optimization algorithms like branch and bound to directly boost downstream task performance, and adapting the method for high-dimensional/structured data to increase applicability in complex settings like energy systems.

## References

Stephen P Boyd and Lieven Vandenberghe. *Convex optimization*. Cambridge university press, 2004.

Arthur M Geoffrion. Lagrangean relaxation for integer programming. In *Approaches to integer programming*, pages 82–114. Springer, 2009.

Laurence A Wolsey and George L Nemhauser. *Integer and combinatorial optimization*. John Wiley & Sons, 1999.

Vladimir Vovk, Alexander Gammerman, and Glenn Shafer. *Algorithmic learning in a random world*, volume 29. Springer, 2005.

Yaniv Romano, Evan Patterson, and Emmanuel Candes. Conformalized quantile regression. *Advances in neural information processing systems*, 32, 2019.

Priya L Donti, David Rolnick, and J Zico Kolter. Dc3: A learning method for optimization with hard constraints. *arXiv preprint arXiv:2104.12225*, 2021.

Wenbo Chen, Mathieu Tanneau, and Pascal Van Hentenryck. End-to-end feasible optimization proxies for large-scale economic dispatch. *IEEE Transactions on Power Systems*, 2023.

Mathieu Tanneau and Pascal Van Hentenryck. Dual lagrangian learning for conic optimization. In *The Thirty-eighth Annual Conference on Neural Information Processing Systems*, 2024. URL <https://openreview.net/forum?id=gN1iKwxIL5>.

Harris Papadopoulos, Kostas Proedrou, Volodya Vovk, and Alex Gammerman. Inductive confidence machines for regression. In *Machine learning: ECML 2002: 13th European conference on machine learning Helsinki, Finland, August 19–23, 2002 proceedings 13*, pages 345–356. Springer, 2002.

Jing Lei, Max G’Sell, Alessandro Rinaldo, Ryan J Tibshirani, and Larry Wasserman. Distribution-free predictive inference for regression. *Journal of the American Statistical Association*, 113(523):1094–1111, 2018.

Anastasios N Angelopoulos and Stephen Bates. A gentle introduction to conformal prediction and distribution-free uncertainty quantification. *arXiv preprint arXiv:2107.07511*, 2021.

Roberto I Oliveira, Paulo Orenstein, Thiago Ramos, and Joao Vitor Romano. Split conformal prediction and non-exchangeable data. *Journal of Machine Learning Research*, 25(225):1–38, 2024.

Chirag Gupta, Arun K Kuchibhotla, and Aaditya Ramdas. Nested conformal prediction and quantile out-of-bag ensemble methods. *Pattern Recognition*, 127:108496, 2022.

Andrei Broder and Michael Mitzenmacher. Network applications of bloom filters: A survey. *Internet mathematics*, 1(4):485–509, 2004.

Amit Goyal, Hal Daumé III, and Graham Cormode. Sketch algorithms for estimating point queries in nlp. In *Proceedings of the 2012 joint conference on empirical methods in natural language processing and computational natural language learning*, pages 1093–1103, 2012.

Graham Cormode, Somesh Jha, Tejas Kulkarni, Ninghui Li, Divesh Srivastava, and Tianhao Wang. Privacy at scale: Local differential privacy in practice. In *Proceedings of the 2018 International Conference on Management of Data*, pages 1655–1658, 2018.

Qingpeng Zhang, Jason Pell, Rosangela Canino-Koning, Adina Chuang Howe, and C Titus Brown. These are not the k-mers you are looking for: efficient online k-mer counting using a probabilistic data structure. *PloS one*, 9(7):e101271, 2014.

Matteo Sesia, Stefano Favaro, and Edgar Dobriban. Conformal frequency estimation using discrete sketched data with coverage for distinct queries. *Journal of Machine Learning Research*, 24(348):1–80, 2023.

Moses Charikar, Kevin Chen, and Martin Farach-Colton. Finding frequent items in data streams. In *International Colloquium on Automata, Languages, and Programming*, pages 693–703. Springer, 2002.

Graham Cormode and Shan Muthukrishnan. An improved data stream summary: the count-min sketch and its applications. *Journal of Algorithms*, 55(1):58–75, 2005.

Ruiting Liang, Wanrong Zhu, and Rina Foygel Barber. Conformal prediction after efficiency-oriented model selection. *arXiv preprint arXiv:2408.07066*, 2024.

Yachong Yang and Arun Kumar Kuchibhotla. Selection and aggregation of conformal prediction sets. *Journal of the American Statistical Association*, pages 1–13, 2024.

Matteo Sesia and Emmanuel J Candès. A comparison of some conformal quantile regression methods. *Stat*, 9(1):e261, 2020.

Guancheng Qiu, Mathieu Tanneau, and Pascal Van Hentenryck. Dual conic proxies for ac optimal power flow. *Electric Power Systems Research*, 236:110661, 2024.

Michael Klamkin, Mathieu Tanneau, and Pascal Van Hentenryck. Dual interior-point optimization learning. *arXiv preprint arXiv:2402.02596*, 2024.

Wenbo Chen, Mathieu Tanneau, and Pascal Van Hentenryck. Real-time risk analysis with optimization proxies. *Electric Power Systems Research*, 235:110822, 2024.

University of Washington, Dept. of Electrical Engineering. Power systems test case archive, 1999. URL <http://www.ee.washington.edu/research/pstca/>.

Stéphane Fliscounakis, Patrick Panciatici, Florin Capitanescu, and Louis Wehenkel. Contingency ranking with respect to overloads in very large power systems taking into account uncertainty, preventive, and corrective actions. *IEEE Transactions on Power Systems*, 28(4):4909–4917, 2013.

Eliana Vivas, Héctor Allende-Cid, and Rodrigo Salas. A systematic review of statistical and machine learning methods for electrical power forecasting with reported mape score. *Entropy*, 22(12):1412, 2020.

Wen-Chuan Wang, Kwok-Wing Chau, Chun-Tian Cheng, and Lin Qiu. A comparison of performance of several artificial intelligence methods for forecasting monthly discharge time series. *Journal of hydrology*, 374(3-4):294–306, 2009.

J Carpentier. Contribution to the economic dispatch problem. *Bulletin de la Societe Francoise des Electriciens*, 3(8):431–447, 1962.

Mathieu Tanneau and Michael Klamkin. PGLearn.jl: A benchmark suite for optimal power flow problems. <https://github.com/AI4OPT/PGLearn.jl>, 2024.

Q. Huangfu and J. A. J. Hall. Parallelizing the dual revised simplex method. *Mathematical Programming Computation*, 10(1):119–142, 2018. doi: 10.1007/s12532-017-0130-5.

Sogol Babaieejadsarookolaee, Adam Birchfield, Richard D Christie, Carleton Coffrin, Christopher DeMarco, Ruisheng Diao, Michael Ferris, Stephane Fliscounakis, Scott Greene, Renke Huang, et al. The Power Grid Library for benchmarking AC optimal power flow algorithms. *arXiv preprint arXiv:1908.02788*, 2019.

Michael Klamkin. ML4OPF: Machine learning for optimal power flow. <https://github.com/AI4OPT/ML4OPF>, 2024.

Adam Paszke et al. PyTorch: An Imperative Style, High-Performance Deep Learning Library. In H. Wallach, H. Larochelle, A. Beygelzimer, F. d’Alché Buc, E. Fox, and R. Garnett, editors, *Advances in Neural Information Processing Systems 32*, pages 8024–8035. Curran Associates, Inc., 2019.

William Falcon and The PyTorch Lightning team. PyTorch Lightning, March 2019. URL <https://github.com/Lightning-AI/lightning>.

## A Proofs for Section 3 (CP With Upper And Lower Bounds)

**Proposition 1.** Let  $\hat{C}(\cdot)$  denote a prediction interval with coverage  $1 - \alpha$ , i.e.,  $\mathbb{P}(Y_{N+1} \in \hat{C}(X_{N+1})) = 1 - \alpha$  for some  $\alpha \in [0, 1]$ . Next, define the strengthened interval  $\tilde{C}(x) := \hat{C}(x) \cap [\hat{B}^l(x), \hat{B}^u(x)]$ ,  $\forall x \in \mathcal{X}$ . Then,  $\mathbb{P}(Y_{N+1} \in \tilde{C}(X_{N+1})) = \mathbb{P}(Y_{N+1} \in \hat{C}(X_{N+1})) = 1 - \alpha$ .

*Proof.* It suffices to prove that  $\mathbb{P}(Y \in \tilde{C}(X)) = \mathbb{P}(Y \in \hat{C}(X))$ . First note that

$$\begin{aligned}\hat{C}(X) &= \hat{C}(X) \cap \mathbb{R} \\ &= \hat{C}(X) \cap ((-\infty, \hat{B}^l(X)) \cup [\hat{B}^l(X), \hat{B}^u(X)]) \cup (\hat{B}^u(X), +\infty)\end{aligned}$$

and note that  $(-\infty, \hat{B}^l(X))$ ,  $[\hat{B}^l(X), \hat{B}^u(X)]$  and  $(\hat{B}^u(X), +\infty)$  are disjoint. Also note that

$$\mathbb{P}(Y \in \hat{C}(X) \cap (-\infty, \hat{B}^l(X))) = \mathbb{P}(Y \in \hat{C}(X) \cap (\hat{B}^u(X), +\infty)) = 0,$$

because  $\hat{B}^l(X) \leq Y \leq \hat{B}^u(X)$  by definition of  $\hat{B}^l, \hat{B}^u$ . It then follows that

$$\begin{aligned}\mathbb{P}(Y \in \hat{C}(X)) &= \mathbb{P}(Y \in \hat{C}(X) \cap (-\infty, \hat{B}^l(X))) + \mathbb{P}(Y \in \hat{C}(X) \cap [\hat{B}^l(X), \hat{B}^u(X)]) \\ &\quad + \mathbb{P}(Y \in \hat{C}(X) \cap (\hat{B}^u(X), +\infty)) \\ &= 0 + \mathbb{P}(Y \in \hat{C}(X) \cap [\hat{B}^l(X), \hat{B}^u(X)]) + 0 \\ &= \mathbb{P}(Y \in \tilde{C}(X))\end{aligned}$$

which concludes the proof.  $\square$

**Theorem 1.** Consider a family of nested prediction sets  $\{\hat{C}_t\}_{t \in \mathcal{T}}$ , where  $\mathcal{T} \subseteq \mathbb{R}$ , and let  $\hat{\tau}$  be obtained following the NCP calibration step as per Eq. (11). Next, define the family of nested strengthened intervals  $\{\tilde{C}_t\}_{t \in \mathcal{T}}$ , where  $\forall x \in \mathbb{R}^d, \forall t \in \mathcal{T}, \tilde{C}_t(x) = \hat{C}_t(x) \cap [\hat{B}^l(x), \hat{B}^u(x)]$ , and let  $\tilde{\tau}$  be obtained from Eq. (11). Then,  $\hat{\tau} = \tilde{\tau}$  and  $\forall x \in \mathbb{R}^d, \hat{C}_{\hat{\tau}}(x) \cap [\hat{B}^l(x), \hat{B}^u(x)] = \tilde{C}_{\tilde{\tau}}(x)$ . (15)

*Proof.* First note that  $\{\tilde{C}_t\}_{t \in \mathcal{T}}$  is indeed a family of nested intervals that satisfies the NCP assumptions; this follows from the fact that  $\tilde{C}_t \subseteq \hat{C}_t, \forall t$ .

Next, using the same argument as the proof of Proposition 1,

$$\forall i \in \mathcal{I}_{\text{cal}}, \mathbf{1}_{\hat{C}_t(X_i)}(Y_i) = \mathbf{1}_{\tilde{C}_t(X_i)}(Y_i) \quad (22)$$

Substituting this in Eq. (11) then yields

$$\left\{ t \left| \sum_{i \in \mathcal{I}_{\text{cal}}} \mathbf{1}_{\tilde{C}_t(X_i)}(Y_i) \geq (1 - \alpha)(1 + |\mathcal{I}_{\text{cal}}|) \right. \right\} = \left\{ t \left| \sum_{i \in \mathcal{I}_{\text{cal}}} \mathbf{1}_{\hat{C}_t(X_i)}(Y_i) \geq (1 - \alpha)(1 + |\mathcal{I}_{\text{cal}}|) \right. \right\}, \quad (23)$$

$\square$

## B Experiment Details

### B.1 Problem formulations

With a slight abuse of notation for the readability, here equality constraints are written out explicitly. Let  $\mathbf{S}(x)$  denote the feasible set of, i.e,

$$\mathbf{S}(x) = \{s \in \mathbb{R}^n | g_x(s) \leq 0, h_x(s) = 0\}$$

A candidate solution  $s \in \mathbb{R}^n$  is *primal feasible* if  $s \in \mathbf{S}(x)$ , i.e., if  $g_x(s) \leq 0$  and  $h_x(s) = 0$ , otherwise it is *infeasible*. Suppose that there exists a unique optimal solution  $x^*$ . Then,  $f_x(x^*) \leq f_x(s)$  for all  $s \in \mathbf{S}(x)$ .

The Lagrangian is defined as:

$$\mathcal{L}(s, \lambda, \mu) = f_x(s) + \lambda^T g_x(s) + \mu^T h_x(s), \quad (24)$$

where  $\lambda \in \mathbb{R}^m$  and  $\mu \in \mathbb{R}^p$  are Lagrange multipliers. Its corresponding dual problem is defined as

$$\varphi(x) = \max_{\lambda, \mu} \inf_s \mathcal{L}(s, \lambda, \mu) \quad (25a)$$

$$\text{s.t. } \lambda \geq 0 \quad (25b)$$

Dual feasibility is defined similarly to primal feasibility,  $\Lambda(\lambda) = \{\lambda \in \mathbb{R}^m | \lambda \geq 0\}$ . Suppose there exists a unique optimal dual solution  $(\lambda_x, \mu_x)$ . By the weak duality theorem, we must have  $\Phi(x) \geq \varphi(x)$ .

**Economic Dispatch** The experiments evaluate the proposed methods in the context of the Optimal Power Flow (OPF) problem Carpentier [1962], a fundamental challenge in power system operations that focuses on optimizing generation dispatch while satisfying various physical and engineering constraints. Specifically, we address the Economic Dispatch problem with soft thermal constraints. In this section, we present the exact mathematical formulations used for learning the primal and dual proxies, following Chen et al. [2023], Klamkin et al. [2024].

Primal formulation (equivalent to “EconomicDispatch” with “soft\_thermal\_limit” enabled in Tanneau and Klamkin [2024]):

$$\min_{p, f, \xi} c^T p + M e^T \xi \quad (26a)$$

$$\text{s.t. } e^T p = e^T d \quad [\lambda] \quad (26b)$$

$$\Phi A_g p - f = \Phi A_d d \quad [\pi] \quad (26c)$$

$$f + \xi \geq \underline{f} \quad [\underline{\mu}] \quad (26d)$$

$$-f + \xi \geq -\bar{f} \quad [\bar{\mu}] \quad (26e)$$

$$\underline{p} \leq p \leq \bar{p} \quad [\underline{z}, \bar{z}] \quad (26f)$$

$$\xi \geq 0 \quad [y] \quad (26g)$$

where  $p$  is the vector of generation,  $d$  is the vector of demand, and  $f$  is the vector of power flows. The vector  $\xi \in \mathbb{R}^E$  denotes the vector of thermal violations. Matrix  $\Phi \in \mathbb{R}^{E \times N}$  is the nodal PTDF matrix,  $A_g \in \mathbb{R}^{N \times G}$  is the incidence matrix of generators, and  $A_d \in \mathbb{R}^{N \times D}$  is the incidence matrix of loads.

The dual problem reads

$$\max_{\lambda, \pi, \mu} \lambda e^T d + (\Phi A_d d)^T \pi + \underline{f}^T \mu - \bar{f}^T \bar{\mu} + \underline{p}^T \underline{z} - \bar{p}^T \bar{z} \quad (27a)$$

$$\text{s.t. } \lambda e + (\Phi A_g)^T \pi + \underline{z} - \bar{z} = c \quad (27b)$$

$$- \pi + \underline{\mu} - \bar{\mu} = 0 \quad (27c)$$

$$\underline{\mu} + \bar{\mu} + y = M e \quad (27d)$$

$$\underline{\mu}, \bar{\mu}, \underline{z}, \bar{z}, y \geq 0 \quad (27e)$$

## B.2 Data generation

Note that all CP methods require true labels to compute exact residuals during the calibration step (11), and the test set must be labeled as well for performance evaluation. These true labels are computed using the LP solver HiGHS Huangfu and Hall [2018], via PGLearn Tanneau and Klamkin [2024]. For the significantly larger training set  $\mathcal{D}_{\text{train}}$ , true labels are not required, as the training process is self-supervised. The three datasets used in this study are based on selected snapshots from the Power Grid Lib - Optimal Power Flow collection Babaeinejadsarookolaee et al. [2019]. The sampling distribution is consistent across all cases. For each sample  $i$ , each load  $d_i$  is generated as

$$d_i^{(i)} = \alpha^{(i)} \beta_i^{(i)} d_i^0,$$

where  $\alpha^{(i)}$  represents a “global” factor and  $\beta_l^{(i)}$  is a “local” factor. The global factor  $\alpha^{(i)}$  follows a Uniform(0.6, 1.0) distribution for 89\_pegase and 118\_ieee, and a Uniform(0.8, 1.05) distribution for 1354\_pegase. The local factor  $\beta_l^{(i)}$  is sampled from Uniform(0.85, 1.15) in all cases. Each snapshot is described next.

### B.2.1 89\_pegase

This case accurately represents the size and complexity of a portion of the European high-voltage transmission network. The network comprises 89 buses, 12 generators, and 210 branches, operating at 380, 220, and 150 kV. The data originate from the Pan European Grid Advanced Simulation and State Estimation (PEGASE) project, which was part of the 7th Framework Program of the European Union Fliscounakis et al. [2013].

### B.2.2 118\_ieee

The test case represents a standard benchmark in power systems engineering, modeling a large-scale electric grid inspired by the American Electric Power system in the Midwestern United States as of December 1962. It includes 118 buses, multiple generators, loads, and transmission lines, and is extensively used by researchers to analyze power system operations under various conditions University of Washington, Dept. of Electrical Engineering [1999].

### B.2.3 1354\_pegase

The data originate from the Pan European Grid Advanced Simulation and State Estimation (PEGASE) project, which is part of the 7th Framework Program of the European Union. This case accurately represents the size and complexity of a segment of the European high voltage transmission network. The network comprises 1,354 buses, 260 generators, and 1,991 branches, operating at 380 and 220 kV Fliscounakis et al. [2013].

## B.3 Optimization proxies (base models)

Optimization proxies are efficient and scalable neural network (NN) models that approximate the input-output mapping of optimization solvers. For instance, when using NN models,  $\theta$  denotes the weights of the NN. Predicting an optimal solution for the primal problem consists of training a model  $\hat{\mathcal{M}}_\theta^p(x) = \hat{s} \in \mathbb{R}^n$  such that  $\hat{s}$  is approximating the true optimal solution of the problem parameterized by  $x$ . Denote the corresponding estimated primal objective value as  $\hat{\Phi}(x) = f(\hat{\mathcal{M}}_\theta^p(x))$ ; similarly, the estimated dual objective value is denoted  $\hat{\varphi}(x) = \inf_s \mathcal{L}(s, \hat{\mathcal{M}}_\theta^d(x))$ .

In this paper, all the primal proxies  $\hat{\mathcal{M}}_\theta^p(x)$  are assumed to be primal-feasible, and all the dual proxies are assumed to be dual-feasible. The predicted objective values  $\{\hat{\Phi}(X_i)\}_{i \in I_{cal} \cup I_{test}}$  and  $\{\hat{\varphi}(X_i)\}_{i \in I_{cal} \cup I_{test}}$  are recovered from the proxies by evaluating (26a) and (27a), respectively. Note that, by the duality theorem, for all  $i \in I_{cal}$ , the following must hold:

$$\hat{\Phi}(X_i) \leq \Phi(X_i) \leq \hat{\varphi}(X_i).$$

To ensure feasibility, the following strategies are employed, as detailed in the subsequent subsections.

### B.3.1 Primal feasible proxies

A primal-feasible solution to 26 can be obtained by following the procedure below, similar to Chen et al. [2023]:

1. Predict  $\tilde{p} \in [\underline{p}, \bar{p}]^G$ .
2. Use the power balance layer [Chen et al., 2023, Eq. 4] to obtain  $p$  from  $\tilde{p}$  such that  $e^\top p = e^\top d$  and  $\underline{p} \leq p \leq \bar{p}$ .
3. Recover  $f = \Phi A_g p - \Phi A_d d$
4. Recover  $\xi = \max(\max(0, f - \bar{f}), \max(0, \underline{f} - f))$

Table 2: Proxy Configurations and Performance Metrics

Dataset	Proxy	#Layers	#Units per Layer	Learning Rate	Decay (Rate/Steps)	MAPE (%)
89_pegase	Primal	3	128	0.001	0.9 / 15	0.23
	Dual	4	128	0.05	0.7 / 15	0.18
118_ieee	Primal	3	256	0.05	0.9 / 20	0.19
	Dual	4	256	0.05	0.7 / 15	0.10
1354_pegase	Primal	4	2048	0.001	0.75 / 15	3.06
	Dual	4	2048	0.0001	0.85 / 10	0.97

### B.3.2 Dual feasible proxies

The Dual Lagrangian Learning framework Tanneau and Hentenryck [2024] is applied; the specific dual recovery procedure reads as follows:

1. Predict  $\lambda \in \mathbb{R}$  and  $\pi \in [-M, M]^E$ .
2. Recover  $\underline{\mu} = \max(0, \pi)$  and  $\bar{\mu} = \max(0, -\pi)$
3. Set  $z = c - \lambda e - (\Phi A_g)^\top \pi$
4. Recover  $\underline{z} = \max(0, z)$  and  $\bar{z} = \max(0, -z)$

### B.3.3 Details of training

Both proxies are trained using the self-supervised approach outlined in Chen et al. [2023], Tanneau and Hentenryck [2024], Klamkin et al. [2024]. The network architecture is a feed-forward network with softplus activations and a 5% dropout rate. The model training is implemented using the ML4OPF Klamkin [2024] library which itself is based on PyTorch Paszke et al. [2019] and Lightning Falcon and The PyTorch Lightning team [2019]. Comprehensive hyperparameter tuning is performed, optimizing learning rate, decay strategy, and model architecture, with the best configuration selected. The optimal hyper parameters are presented in Table 2.

For all datasets, both the primal and dual proxies are implemented using the *softplus* activation function. The configurations and performance metrics are summarized in Table 2.

Note that the hyperparameters for 1354\_pegase result in a relatively high primal MAPE, primarily due to the sensitivity of optimal hyperparameters in one of the ten splits, which reflects a commonly observed challenge in robust hyperparameter tuning within deep learning.

## B.4 Experiment Details

All experiments are conducted on RHEL9 machines with 24 Intel Xeon 2.7 GHz CPU cores, equipped with an NVIDIA V100 GPU. Random shuffling and splitting of data samples is performed separately for each dataset. The process is repeated 10 times for statistical reliability of the results, and the average and standard deviation of the results are reported. For each round, 40,000 samples are used for training, 5,000 for calibration, and 5,000 for testing, ensuring robust evaluation.

### B.4.1 Details of comparison methods

CPUL and its optimized version, CPUL-OMLT, are compared against three other CP methods. For clarity, the construction of all methods used in the experiments is summarized in Table ??.

The first comparison method is the widely applied Split CP Vovk et al. [2005], as reviewed in Section 2. With two base models,  $\hat{B}^u$  and  $\hat{B}^l$ , classical CP is independently applied to each model. Specifically, the unsigned residuals  $\hat{s}^u(x, y) = y - \hat{B}^u(x)$  and  $\hat{s}^l(x, y) = y - \hat{B}^l(x)$  serve as score functions to capture residual distribution differences between  $\hat{B}^u$  and  $\hat{B}^l$ . When a single base model constructs prediction intervals, the other is incorporated via a post-processing step, as described in (14), aligning the Split CP constructions with CPUL-u and CPUL-l.

The second category of comparison focuses on CQR methods Romano et al. [2019], Sesia and Candès [2020]. In the adopted versions, the fitted quantile estimates are replaced with the base models: the

upper quantile is substituted with  $\hat{B}^l$  and the lower quantile with  $\hat{B}^u$ . For CQR-r, an additional scaling factor of  $1/(\hat{B}^u - \hat{B}^l)$  is applied.

#### B.4.2 OMLT implementation details

Note that OMLT requires optimizing the parameter  $\ell$ . In the paper's implementation, this is achieved by performing a grid search on  $\ell$ . This grid search is performed using 1000 samples, reserved from the calibration set. For each CPUL submethod, choose a hyper-parameter  $\ell$  using the following strategy. For each  $\ell$  in the search space, (21) is solved by applying (11) to the reserved 1000 samples at the confidence level of  $1 - \alpha$  coverage. The optimal  $\ell$  is selected based on the average prediction interval length at the given  $1 - \alpha$  level on the hold-out set of 1,000 samples. Then, each CPUL submethod with the optimal  $\ell$ , calibration (and model-selection) is conducted using the remaining 4,000 samples. Lastly, CPUL-OMLT is verified on the test set.

Table 3: Comparisons of CP Methods Across Different Datasets: 89\_pegase, 118\_ieee, and 1354\_pegase.

UQ Methods	$\alpha = 2.5\%$		$\alpha = 5\%$		$\alpha = 7.5\%$		$\alpha = 10\%$		$\alpha = 12.5\%$		$\alpha = 15\%$	
	PICP (%)	Length (%)	PICP (%)	Length (%)	PICP (%)	Length (%)	PICP (%)	Length (%)	PICP (%)	Length (%)	PICP (%)	Length (%)
89_pegaso												
$[\hat{B}^t, \hat{B}^u]$	100.0 (0.00)	0.410 (0.016)	100.0 (0.00)	0.410 (0.016)	100.0 (0.00)	0.410 (0.016)	100.0 (0.00)	0.410 (0.016)	100.0 (0.00)	0.410 (0.016)	100.0 (0.00)	0.410 (0.016)
Split CP w/ $\hat{B}^t$	97.56(0.28)	<b>0.281 (0.027)</b>	95.02(0.40)	<b>0.242 (0.026)</b>	92.61(0.57)	<b>0.218 (0.015)</b>	90.15(0.60)	0.197(0.007)	87.91(0.85)	0.188(0.006)	85.50(1.03)	0.181(0.007)
Split CP w/ $\hat{B}^u$	97.57(0.26)	0.260(0.03)	95.02(0.43)	0.230(0.06)	92.40(0.69)	0.215(0.06)	90.02(0.54)	<b>0.205 (0.007)</b>	87.68(0.52)	<b>0.194 (0.008)</b>	85.09(0.44)	<b>0.184 (0.008)</b>
SFD CP	98.18(0.05)	<b>0.239 (0.006)</b>	95.97(0.27)	<b>0.2150 (0.009)</b>	93.61(0.35)	<b>0.1980 (0.007)</b>	91.23(0.56)	<b>0.188 (0.007)</b>	88.85(0.69)	<b>0.1780 (0.006)</b>	86.63(0.84)	<b>0.1670 (0.007)</b>
CQR	98.14(0.50)	<b>0.402 (0.018)</b>	95.95(1.05)	<b>0.398 (0.018)</b>	93.78(1.49)	<b>0.394 (0.018)</b>	91.40(1.80)	<b>0.389 (0.018)</b>	89.54(2.24)	<b>0.384 (0.017)</b>	87.23(2.50)	<b>0.381 (0.017)</b>
CQR-r	97.79(0.40)	<b>0.376 (0.019)</b>	95.37(0.46)	<b>0.359 (0.020)</b>	93.09(0.55)	<b>0.344 (0.020)</b>	90.71(1.72)	<b>0.332 (0.020)</b>	88.24(0.70)	<b>0.319 (0.020)</b>	85.48(0.86)	<b>0.309 (0.019)</b>
CPUL (ours)	98.18(0.05)	<b>0.239 (0.006)</b>	95.97(0.27)	<b>0.2150 (0.009)</b>	93.61(0.35)	<b>0.198 (0.007)</b>	91.23(0.56)	<b>0.188 (0.007)</b>	88.85(0.69)	<b>0.1780 (0.006)</b>	86.63(0.84)	<b>0.1670 (0.007)</b>
CPUL-OMLT (ours)	98.18(0.05)	<b>0.239 (0.006)</b>	95.97(0.27)	<b>0.2150 (0.009)</b>	93.61(0.35)	<b>0.198 (0.007)</b>	92.98(0.51)	<b>0.187 (0.008)</b>	88.80(0.90)	<b>0.175 (0.010)</b>	85.57(1.07)	<b>0.165 (0.009)</b>
118_ieee												
$[\hat{B}^t, \hat{B}^u]$	100.0 (0.00)	0.281 (0.085)	100.0 (0.00)	0.281 (0.085)	100.0 (0.00)	0.281 (0.085)	100.0 (0.00)	0.281 (0.085)	100.0 (0.00)	0.281 (0.085)	100.0 (0.00)	0.281 (0.085)
Split CP w/ $\hat{B}^t$	97.68(0.29)	<b>0.242 (0.149)</b>	95.30(0.48)	<b>0.230 (0.148)</b>	92.75(0.53)	<b>0.2170 (0.147)</b>	90.34(0.60)	<b>0.206 (0.146)</b>	87.78(0.58)	<b>0.196 (0.143)</b>	85.35(0.69)	<b>0.186 (0.143)</b>
Split CP w/ $\hat{B}^u$	97.75(0.15)	<b>0.144 (0.007)</b>	95.39(0.26)	<b>0.1270 (0.005)</b>	92.74(0.50)	<b>0.1150 (0.004)</b>	90.00(0.50)	<b>0.105 (0.004)</b>	87.43(0.55)	<b>0.098 (0.005)</b>	84.92(0.52)	<b>0.091 (0.005)</b>
SFD CP	97.68(0.25)	0.180(0.007)	95.19(0.30)	0.1620(0.008)	92.72(0.47)	0.1460(0.011)	90.10(0.50)	0.135(0.013)	87.56(0.69)	0.125(0.015)	85.13(0.66)	0.118(0.015)
CQR	97.76(0.18)	<b>0.2140 (0.146)</b>	95.57(0.69)	<b>0.2050 (0.147)</b>	93.41(1.16)	<b>0.1980 (0.147)</b>	91.34(1.66)	<b>0.193 (0.147)</b>	90.08(0.75)	<b>0.1900 (0.147)</b>	87.17(2.26)	<b>0.184 (0.148)</b>
CQR-r	97.83(0.40)	<b>0.2600 (0.166)</b>	95.62(0.78)	<b>0.1960 (0.168)</b>	93.05(0.92)	<b>0.1870 (0.169)</b>	90.88(1.33)	<b>0.1800 (0.167)</b>	89.56(2.49)	<b>0.1760 (0.163)</b>	85.86(2.29)	<b>0.1660 (0.167)</b>
CPUL (ours)	97.81(0.18)	<b>0.143 (0.007)</b>	95.45(0.30)	<b>0.1270 (0.005)</b>	92.83(0.53)	<b>0.1150 (0.005)</b>	90.02(0.46)	<b>0.105 (0.004)</b>	87.43(0.53)	<b>0.0980 (0.005)</b>	85.01(0.53)	<b>0.0910 (0.005)</b>
CPUL-OMLT (ours)	97.77(0.15)	<b>0.143 (0.008)</b>	95.41(0.23)	<b>0.1260 (0.006)</b>	92.78(0.56)	<b>0.1140 (0.006)</b>	90.01(0.48)	<b>0.103 (0.007)</b>	87.50(0.59)	<b>0.0950 (0.006)</b>	84.93(0.62)	<b>0.0890 (0.006)</b>
1354_pegaso												
$[\hat{B}^t, \hat{B}^u]$	100.0 (0.00)	3.949 (3.807)	100.0 (0.00)	3.949 (3.807)	100.0 (0.00)	3.949 (3.807)	100.0 (0.00)	3.949 (3.807)	100.0 (0.00)	3.949 (3.807)	100.0 (0.00)	3.949 (3.807)
Split CP w/ $\hat{B}^t$	97.31(0.35)	<b>1.560 (1.267)</b>	94.64(0.32)	<b>1.324 (1.212)</b>	92.05(0.40)	<b>1.363 (1.186)</b>	89.60(0.54)	<b>1.308 (1.160)</b>	87.07(0.76)	<b>1.262 (1.135)</b>	84.64(0.69)	<b>1.225 (1.123)</b>
Split CP w/ $\hat{B}^u$	97.14(0.31)	<b>3.568 (3.837)</b>	94.66(0.32)	<b>2.680 (2.724)</b>	92.15(0.48)	<b>2.207 (2.678)</b>	89.40(0.49)	<b>1.570 (0.853)</b>	87.03(0.57)	1.073(0.32)	84.75(0.55)	<b>0.686 (0.098)</b>
SFD CP	97.45(0.10)	2.975(2.598)	95.01(0.25)	2.324(2.037)	92.38(0.21)	1.741(2.180)	90.22(0.27)	1.456(0.609)	87.74(0.45)	<b>0.370 (0.069)</b>	85.09(0.51)	0.718(0.050)
CQR	97.24(0.32)	<b>3.590 (3.947)</b>	94.75(0.36)	<b>3.552 (3.943)</b>	92.45(0.40)	<b>3.524 (3.942)</b>	90.13(0.43)	<b>3.501 (3.939)</b>	87.54(0.62)	<b>3.480 (3.069)</b>	84.87(0.74)	<b>3.461 (3.937)</b>
CQR-r	97.48(0.31)	<b>3.570 (3.870)</b>	95.37(0.36)	<b>3.406 (3.947)</b>	92.01(0.38)	<b>3.322 (3.981)</b>	91.57(0.52)	<b>3.273 (3.997)</b>	87.99(2.12)	<b>3.234 (3.008)</b>	88.25(0.39)	<b>3.212 (2.046)</b>
CPUL (ours)	97.25(0.28)	<b>1.554 (1.275)</b>	94.62(0.33)	<b>1.321 (1.215)</b>	92.14(0.42)	<b>1.360 (1.189)</b>	89.65(0.56)	<b>1.306 (1.162)</b>	87.74(0.43)	<b>0.837 (0.069)</b>	84.80(0.57)	<b>0.632 (0.048)</b>
CPUL-OMLT (ours)	97.31(0.20)	<b>1.205 (1.275)</b>	94.66(0.42)	<b>1.108 (1.202)</b>	89.69(0.50)	<b>0.370 (0.089)</b>	87.74(0.43)	<b>0.370 (0.069)</b>	85.68(0.52)	<b>0.642 (0.040)</b>		

\* For each dataset and  $\alpha$  value, the three shortest intervals are colored blue, while the three largest intervals are colored red.

## C Additional experiment results

See additional details of experiments given in Table 3.